A PROPELLER-INTEGRATION STUDY COMPARING EXPERIMENTAL DATA WITH NUMERICAL FLOW SOLUTIONS BASED ON THE NAVIER-STOKES EQUATIONS

L.L.M. Veldhuis
Delft University of Technology, Dept. of Aerospace Engineering
Kluyverweg 1, 2629 HS Delft, the Netherlands

S. Nebiolo
Polytechnico di Torino
Department of Aerospace Engineering
Corso Duca Degli Abruzzi, 24, 10129 Torino - Italy

Abstract

Navier-Stokes calculations were performed on a low aspect ratio straight semi-span wing equipped with a four bladed tractor propeller. The total number of grid cells that was used during the calculations is close to 1 million. The flow problem was solved using a cell-centered finite volume approach, using various turbulence models that were compared with each other. The Realizable k-ε and the Reynolds Stress Model with non-equilibrium wall functions showed the best results for this particular flow field. The calculations were aimed at the prediction of the complex flow field around propeller-wing configuration were used to determine the minimum grid size and problem setup that is needed to acquire acceptable results without having to use the most powerful supercomputers available.
The results are compared with experimental data acquired with a low speed windtunnel model. Detailed post-processing of the numerical data produced an improved understanding of the aerodynamic phenomena that occur at the part of wing that is washed by the slipstream. The overall characteristics like the lift coefficient and the drag show an reasonable agreement between the data. The choice, however, of the selected turbulence model as well as the boundary conditions set at the propeller disk are of vital importance. This again signifies the importance of experiments on this particular complex flow field.

Symbols

A	wing aspect ratio
b	wing span
c	local chord
c_d	local drag coefficient
c_l	local lift coefficient
C_L	total lift coefficient of the configuration
C_N	normal force coefficient
D	drag force, propeller diameter
f	source function used in the QWS-method
F, G	functions used in the QWS-method
p	static pressure
p_t	total pressure
S	wing area
S_1, S_2	windtunnel cross sectional areas
T	thrust force, temperature
T_c	Thrust coefficient ($= T/\rho V^2 D^2$)
u, v, w	x,y and z-component of the velocity vector
x, y, z	coordinates in streamwise, spanwise and vertical direction respectively
α	geometrical angle of attack
α_i	induced angle of attack
φ	velocity-potential-like function used in the QWS-method

ψ streamfunction-like function used in the QWS-method
ρ air density

Indices

c.l. center line
p propeller
ref reference value
v viscous
w wing
QWS Quantitative Wake Survey

1 Introduction

For multi-engined propeller powered aircraft one of the important points of concern with respect to the overall performance is the interaction between the propeller slipstream and the wing. In tractor propeller configurations the trailing wing experiences swirl velocities generated by the propeller which results in a considerable deformation of the lift distribution. This has a significant impact on the aerodynamic behavior and performance of the wing. Within various European research projects specific attention was paid to the analysis rather than the optimization of current concepts. It would be interesting however to investigate new design strategies as well. From earlier investigations it is known, that both the position of the powerplant with respect to the wing and propeller angle of attack play an important role (ref. [1-5]). Consequently carefully designed configurations may reveal some performance benefits when the propeller and the wing are closely coupled. To arrive at optimized concepts however further detailed information on the typical flow phenomena around the propeller-wing configuration is needed. The aim of this paper is to present some results of a comparison of numerical calculations based on the Navier-Stokes equations and experimental investigations including flow field surveys and surface pressure measurements that were performed on a basic tractor propeller wing configuration.

2 Experimental Approach

2.1 Windtunnel facility and model

Validation of the numerical calculations was accomplished through experiments on a simple propeller-wing model called PROWIM (propeller wing interference model). Typical model characteristics are summarized in Table 1. The model was attached to an external 6-component balance through a turntable which is flush with the image plate situated at 0.3 m from the upper wall. The windtunnel used during these investigations was the Delft University Low Turbulence Tunnel (LTT) which has an octagonal test section of $L \times W \times H$ = 2.60 x 1.80 x 1.25m. Beside the balance measurements surface pressures were meas-

Model characteristics of windtunnel model PROWIM	
Wing aspect ratio	5.33
Airfoil	NACA 64A015
Span , chord	0.64 m , 0.24 m
Propeller drive power	5.5 kW
Propeller blade angle	25°
Propeller diameter	0.236 m
Features	Inb. / outb. Flaps ; 918 pressure taps
Measurements	External balance ; surface pressure ; 5-hole-probe wake survey
Test conditions	α =0°,4°,10° ; Re = 0.82×10^6 ; prop on / off ; prop on : T_c = 0.168

Table 1 Model characteristics and test conditions of PROWIM.

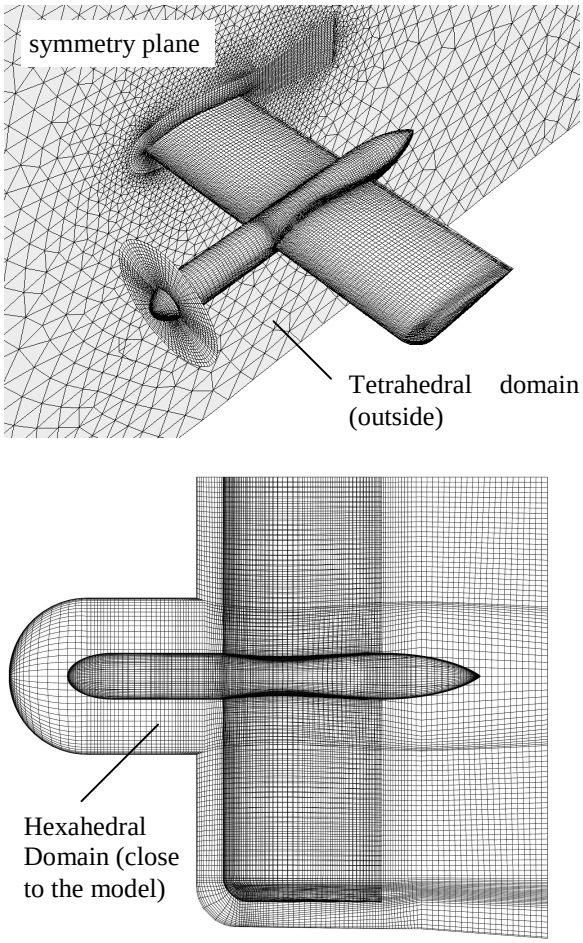

fig. 1 Layout of the numerical model represented by a part of the grid, that was used during the Navier-Stokes calculations.

ured as well as velocity components and pressures in the flowfield. For the wake surveys, that were taken at 1 chord length behind the wing trailing edge, a conical-head five-hole probe (diameter 1.65 mm) was used.

3 Numerical model

The numerical model is based on a somewhat simplified geometry. Instead of a blunt head the spinner is modeled with an elliptically shaped form. This improves the grid quality considerably without violating the general aerodynamic characteristics to much. To capture the complex flow characteristics in the boundary layer and close to the model in the vicinity of the propeller slipstream a rather dense grid was used while the outer calculation domain was rendered with a course grid. To simplify the grid generation process an unstructured hybrid grid approach was used. The cells closest to the wing surface are hexahedrals which perform better in capturing the boundary layer flow phenomena. The cells in the outer domain were less accuracy may be accepted are tetrahedrals. This hybrid approach speeds up the grid generation process considerably. The total number of grid cells that was used during the calculations is approximately 1 million. The flow problem was solved using a cell-centered finite volume approach, using various turbulence models that were compared with each other. The turbulent boundary layer can be subdivided into a inner and a outer region, the first is characterized by having a universal behaviour (the “law of the wall”), the second depends on the pressure distribution and is called “wake region”. The law of the wall can be divided in three regions: the viscous sublayer (extending from the wall to $y^+ \approx 5$), the log-layer (from $y^+ = 30$ to $y^+ = 350$) and the buffer layer (in between). The flow solver provides two approaches to model the near-wall region. The first one is the wall-function approach in which viscous sublayer and buffer layer are not solved, the second is called two-layer zonal model in which the viscous dominated region is solved completely. The two-layer zonal model provides better accuracy for high complexity flows: those flows characterized by high streamline curvatures, high pressure gradients, separation and reattachment, but it requires enough cells in the viscous sublayer. Since it was impossible to have such a fine grid resolution on the model it has been discarded. "Non equilibrium wall functions” were used to be able to account for the effects of pressure gradients giving better accuracy in all those cases in which the flow departs from equilibrium conditions.

Both the so-called Realizable k-ε (RKE) and the Reynolds Stress Model (RSM) with non-equilibrium wall functions that were used showed the best results for this particular flow

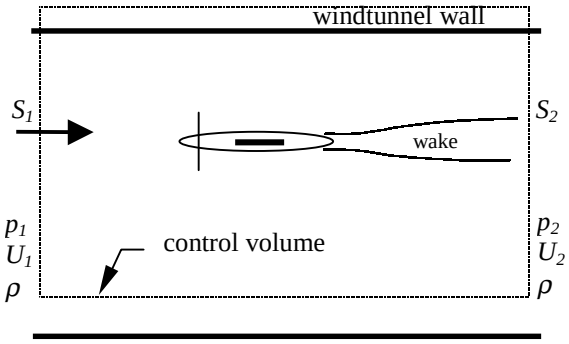

fig. 3 Control volume approach used in the Quantitative-Wake-Survey-Method.

field. An impression of the computational grid is presented in fig. 1.

3.1 Modeling the propeller

The propeller was modeled based on an actuator disk approach. A separate study on a SR3 propfan model by Luursema [[4] showed that this approach is very acceptable when modeling the flow at some distance (the wing position) behind the propeller. The main reason for this is the spreading of vorticity contained in the helical vortices into a tube like structure when the time averaged effect on the wing is considered. The propeller is approximated as an infinitely thin disk with prescribed jump conditions. The jumps in total pressure and swirl velocity that occur over the disk were based on experimental data available from the 5-hole probe experiments performed earlier on the same model. (Rentema [[5]).

4 Quantitative wake survey

One interesting procedure that results in the separate contributions of the profile drag, the induced drag and the lift is the so-called quantitative wake survey method (QWS).
The forces acting the model, that is positioned inside a control volume as depicted in fig. 3, can be found from the change in momentum in the direction of the undisturbed flow. A detailed description of the wake survey method is felt to be beyond the scope of this report. An extensive discussion is given by Maskell [[11], Betz [[10], Rentema [[5], Wu et al.[[12] and Veldhuis [[8].

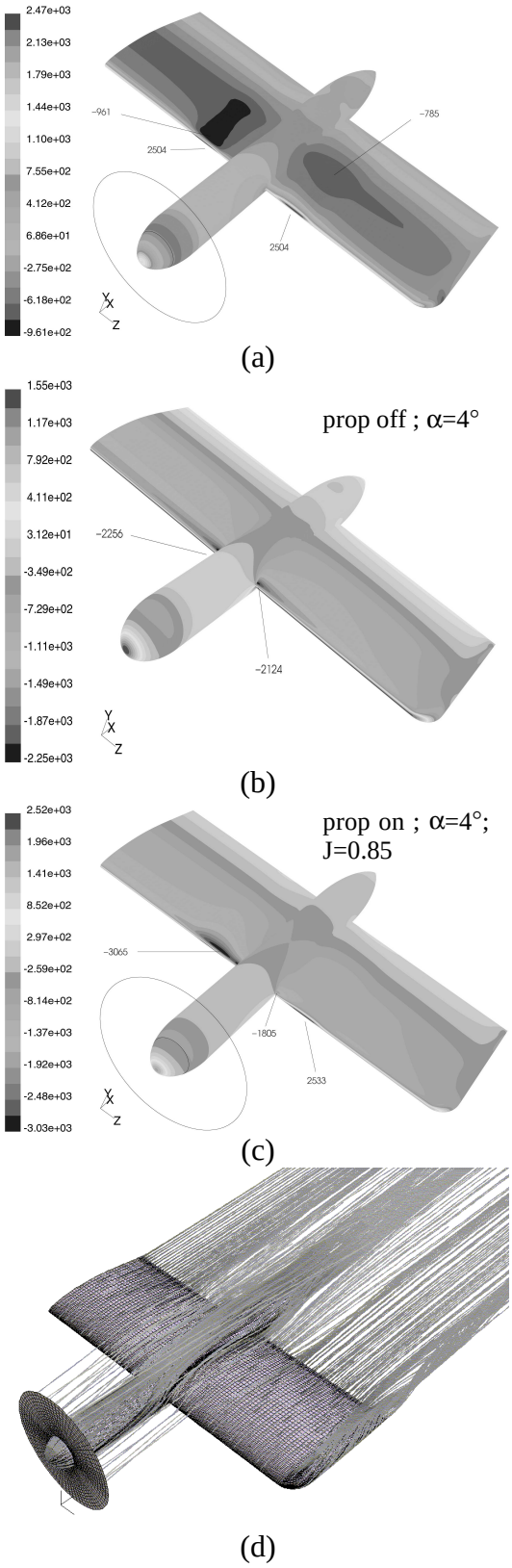

fig. 2 Examples of the surface pressure distributions and the streamline pattern around the propeller wing model showing the propeller slipstream effect and wing tip vortex flow. Angle of attack, α = 4 °, J=0.85.

Summarizing the results of the QWS-method we can state that local lift coefficient and the drag coefficient are integral functions (F,G) of various parameters which may be written as :

$$C_L = \iint F(\xi) \qquad (1)$$

$$C_D = C_{Dp} + C_{Dv} = \iint G(P_t, \varphi, f, \psi, u) \qquad (2)$$

These integrals are taken over the wake at a specified constant streamwise location. In our case the 5-hole probe measurement data were used to provide these parameters.

5 Some calculation results

5.1 Flow field and surface pressures

The experimental investigations were based on external balance and detailed surface pressure measurements. All data were corrected for windtunnel wall effects. Time-averaged slipstream and wake measurements behind the wing were performed using a fast traversing 5 hole probe to analyze slipstream influence on wing profile drag and induced drag. These data provided the baseline information on the flow field characteristics of a single rotation propeller/nacelle/wing configuration. First of all the general flow field of the propeller-wing configuration is presented in fig. 2.

The effects of the propeller slipstream on the wing pressure distribution are clearly visible. Due to the inboard up rotating propeller the stagnation point has moved on both sides of the nacelle and consequently the pressure distributions are influenced (fig. 4). It should be reminded that the pressure distributions, as presented in fig. 2 and fig. 4 are affected both by the local propeller induced flow angles and the dynamic pressure increase in the slipstream. Other phenomena that are clearly visible are : the rotating slipstream and the wing tip vortex.

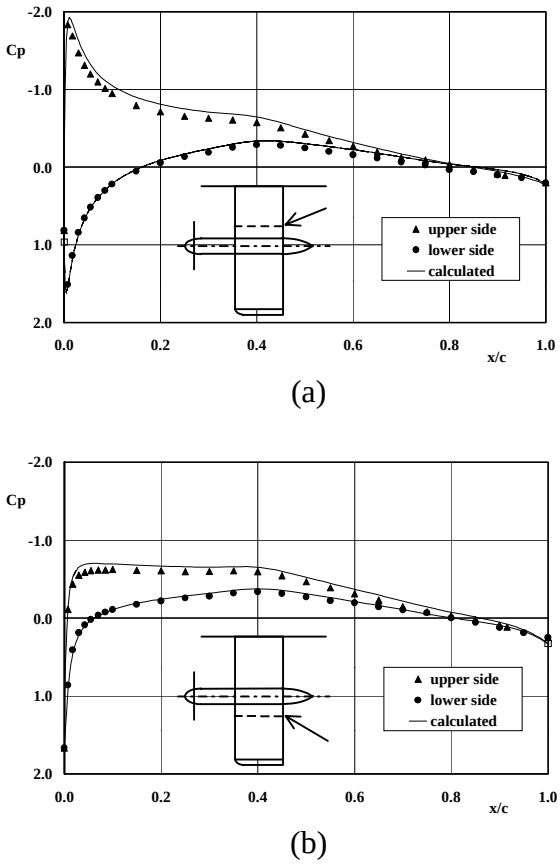

fig. 4 Experimental and calculated pressure distribution at α=4°, prop on. (a) at y/b/2 = 0.345, (b) at y/b/2 = 0.623

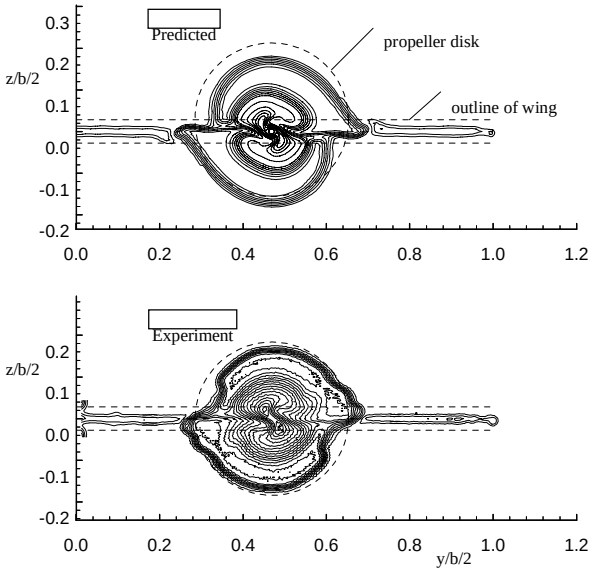

fig. 5 Example of contour lines of constant total pressure coefficient, α = 0°, prop on

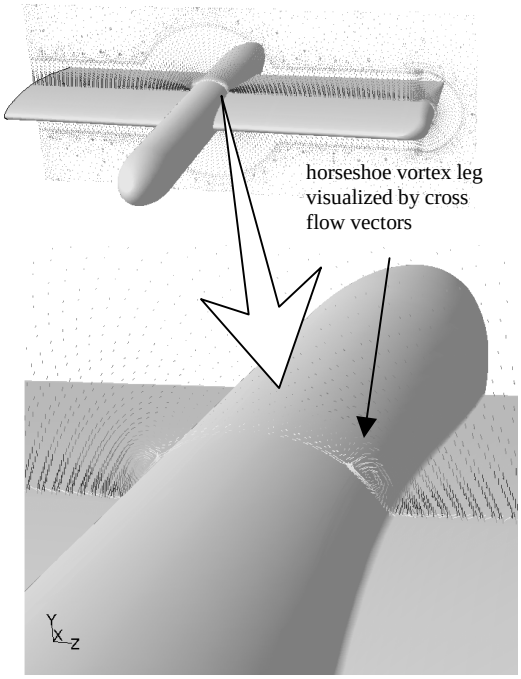

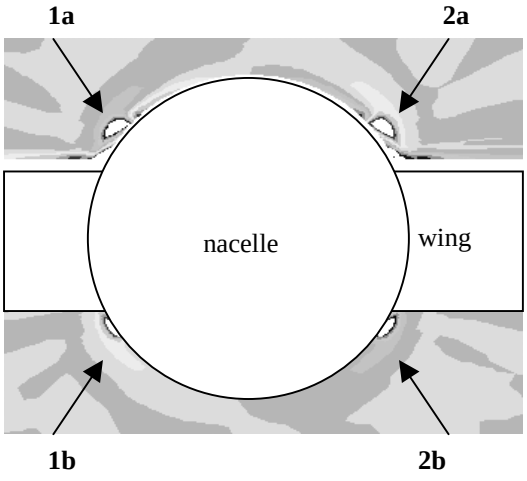

fig. 6 Cross flow vectors and contour plots of axial vorticity close to the nacelle indicating the existence of a horse shoe vortex pair (1ab and 2ab); prop off ; α=0°.

An example of the total head pressure field found from the 5 hole probe experiments and the numerical calculations, respectively is presented in fig. 5. The calculated slipstream and wake show a close resemblance. This is necessary for the quantitative wake analysis to be successful ([[8]]).

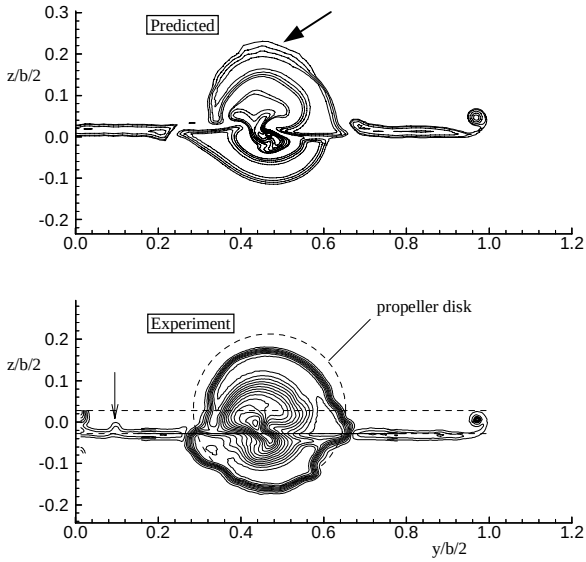

fig. 7 Contour lines of constant total pressure coefficient, α=4°, prop on

As can be seen in fig. 6 the numerical model is capable to predict the major vorticity related flow phenomena like the horseshoe vortex that is produced by the wing-nacelle juncture flow. This is important for the flow considered since the lift distribution that is affected by the propeller slipstream is dominated by the vortical flow effect.
The capturing of thin layers with concentrated vorticity however is very much influenced by the grid density. An example of this is presented in fig. 7 where the total pressure increase produced by the propeller is lost rather quickly (see thick arrow) at the upper side where the hexahedral grid switches over into a tetrahedral grid with much wider cells. When the grid is laid out well however the capturing of the secondary flow vortices, with their associated increase in induced drag, in the calculation model make it possible to optimize the configuration based on these calculations with only limited number of cells (here approximately 1 million).

All the pictures with running propeller show a significant distortion of the slipstream when the wing cuts it in half. The original tube-like shape is replaced by two dislocated segments (see fig. 5). At the location of the cut the slip-

stream is stretched at the side moving away from the wing and compressed at the other side. A convenient explanation of this phenomenon can be found in the way the slipstream influences the wing lift distribution. The contour plot of fig. 8 shows that strong vorticity is shed from the junction of the wing surface and the edge of the slipstream, which is indicative of the high gradient of spanwise load on the wing. As a result both slipstream halves shift in opposite spanwise directions near the intersections between the wing and the slipstream outer boundary.

5.2 Comparison with balance measurements

Table 2 contains some data of the numerical and the experimental wake surveys which are compared with the balance measurements of Philipsen [[6]. Here the coefficient C'_D represents the total streamwise force coefficient :

$$C'_D = C_D - T_c \frac{2D^2}{S} \qquad (3)$$

The results demonstrate an acceptable prediction quality for the NS-calculations.

It is clear that the drag coefficient, C'_D, found in the case of a running propeller includes the thrust component and therefore becomes negative. From Table 2 it can be concluded that the wake survey of the CFD data produce a lift coefficient that is very close to the balance data. For $\alpha = 4°$, both in the case of prop off and prop on, the lift coefficient is (almost) exactly reproduced. The drag data produced are less accurate but still better that the results from the surface integration as shown in Table 3.

In fig. 9 an example a comparison is made between the lift distribution as found from the QWS-method both for the experimental field data (40,000 grid points) and the calculated data

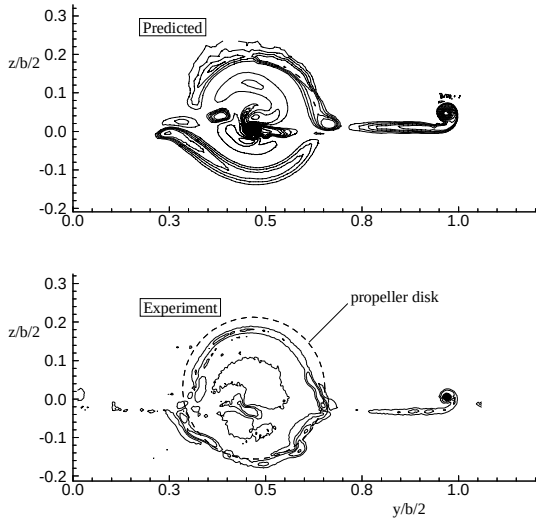

fig. 8 Contour lines of constant axial vorticity, α=4°, prop on.

(5,000 grid points). Minor differences exist over the full span but still the major effects of the slipstream on the spanwise lift distribution become visible. Again this is an indication that the numerically modeled flow field is capable of representing the most important interaction effects between the propeller and the wing.

Method	α	prop	C_L	C'_D
CALC. wake analysis	0	off	0.000	0.0109
	4	off	0.288	0.0171
	0	on	0.003	-0.0985
	4	on	0.310	-0.0910
CALC. surface forces(*)	0	off	0.000	0.0170
	4	off	0.291	0.0231
	0	on	0.004	-0.0926
	4	on	0.319	-0.0857
EXP. wake analysis	0	off	-	-
	4	off	0.292	0.0192
	0	on	0.010	-0.1016
	4	on	0.330	-0.0989
EXP. balance data	0	off	0.000	0.015
	4	off	0.288	0.0198
	0	on	0.006	-0.0986
	4	on	0.314	-0.0916

(*) corrected for thrust contribution

Table 2 Comparison of calculated and measured lift and drag coefficients.

Method	α	prop	$\Delta C'_D$ (%)
CALC. wake analysis	0	off	27.3
	4	off	13.6
	0	on	0.1
	4	on	0.7
CALC. surface forces	0	off	-13.3
	4	off	-16.7
	0	on	6.1
	4	on	6.4

Table 3 Error in estimated drag coefficients with reference to the balance measurements of Philipsen [[6].

Case	C_L	C'_D
in up	0.319	-0.0857
outb. up	0.299	-0.0839

Table 4 Effect of the rotation direction as calculated with NS-solver for $\alpha = 4°$; $J = 0.85$

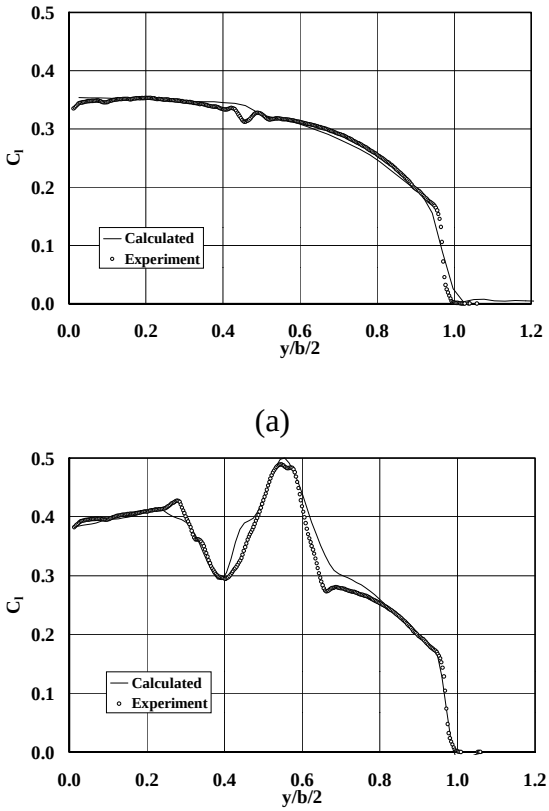

(a)

(b)

fig. 9 Example of measured and calculated lift distributions from wake analysis for α = 4°, (a) prop off, (b) prop on.

Although the flow field surveys produce a drag coefficient that is slightly smaller than the drag from the external balance measurements the agreement between the three techniques is acceptable. Both the numerical and the experimental data are qualitatively and to a lesser extent quantitatively in agreement with the results of an optimization code used for preliminary design purposes that was designed for optimization of propeller-wing configurations.

It has been shown in earlier investigations that the rotation direction has some influence on the overall performance of the propeller-wing configurations ([[1,[6,[3,[10]). In all studies the inboard-up rotating propeller configuration performed slightly better than the outboard-up configuration. Within the numerical model is was very easy to reverse the rotation direction of the propeller and to see whether or not the phenomenon could be confirmed. The calculation was run for $\alpha = 4°$ using the realizable $k-\varepsilon$ model.

In agreement with earlier found experimental evidence the numerical code indeed predicts performance benefits (lower drag combined with higher lift) for configurations that utilize inboard up rotation of the propeller as can be seen in Table 4.

6 Conclusions

From the numerical and experimental investigations the following conclusions can be drawn :

- Applying the Navier-Stokes solver with given boundary conditions, the experimental results, that were attained at low Reynolds number, are acceptably predicted.
- The number of cells used in the current analysis (approx. 1 million) seems to be the bare minimum that is needed to resolve the trailing vorticity field in the wake of the model. Especially the domain

around the slipstream should be provided with a fine grid.

- The numerical results confirm the possible improved efficiency of systems with up-inboard rotation.
- Quantitative wake survey performed in the flowfield behind the propeller deliver results comparable with the experimental flow survey. Thus the CFD-calculation may be an important tool to detect sources of drag on the configuration.
- The final results depend on the turbulence model selected. This again expresses the importance of experimental investigation of this particular complex flow field. Further analysis with adapted turbulence models may be necessary.

References

[1] Veldhuis, L.L.M., Experimental Analysis of Tractor Propeller Effects on a Low Aspect Ratio Semi-Span Wing, Second Pacific International Conference on Aerospace Science and Technology & the Sixth Australian Aeronautical Conference, Vol. 2, p. 491-498, Melbourne, 20-23 march 1995.

[2] Colin, P. ; Moreux, V. ; Barillier, A. , Numerical study of high speed propeller engine integration on transport aircraft, ICAS-96-4.10.1, Sorrento Italy, Sept. 1996

[3] Miranda, L.R. and Brennan, J.E. , Aerodynamic effects of wingtip-mounted propellers and turbines, AIAA 86-1802, 1986

[4] Luursema, G. : Comparison of an actuator disk and a blade modeling approch in Navier-Stokes calculations on the SR-3 propfan, MSc. Thesis, Delft University of Technology, Delft University of Technology, 1999

[5] Rentema, D.W.E., Drag and lift calculations based on wake surveys of a propeller-wing combination at several angles of attack, Graduate thesis, Fac. of Aerospace Engineering, Delft University of Technology, 1994

[6] Philipsen, I., Analysis of Propeller/Wing Interference on a Straight Half Wing and Tractor propeller, Graduate thesis, Fac. of Aerospace Engineering, Delft University of Technology, 1993

[7] Heyma, P.M. , Analysis and Optimization of a Tractor Propeller-wing configuration, TWAIO-thesis, June 1996, Dept. of Aerospace Engineering, Delft University of Technology

[8] Veldhuis, L.L.M. , Experimental analysis of the vortex wake structure behind a propeller-wing configuration, AGARD-CP-584, Conf. proceedings 584, 1996, AGARD Symposium , Trondheim Norway

[9] Lötstedt, P. , Accuracy of a propeller model in inviscid flow, *Journal of Aircraft*, vol. 32, No. 6, nov./dec. 1995

[10] Betz, A., Ein verfahren zur direkten Ermittlung des Profielwiderstandes, *Zeitschrift für Flugtechnik und Motorschiffahrt*, Vol. 16, p.42, 1925

[11] Maskell, E.C., Progress towards a method for the measurement of components of the drag of a wing of finite span, RAE TR-72232, jan. 1973

[12] Wu, J.C., Hackett, J.E., Lilley, D.E., "A generalized wake-integral approach for drag determination in three-dimensional flows", AIAA 79-0279, jan. 1979